





Article

High-Entropy Borides under Extreme Environment of Pressures and Temperatures

Seth Iwan ¹, Chia-Min Lin ¹, Christopher Perreault ¹, Kallol Chakrabarty ¹ , Cheng-Chien Chen ¹ ,
Yogesh Vohra ^{1,*} , Rostislav Hrubciak ², Guoyin Shen ²  and Nenad Velisavljevic ^{2,3}

¹ Department of Physics, University of Alabama at Birmingham, Birmingham, AL 35294, USA; iwanseth@uab.edu (S.I.); lincm@uab.edu (C.-M.L.); cperre@uab.edu (C.P.); kallol89@uab.edu (K.C.); chenc@uab.edu (C.-C.C.)

² High Pressure Collaborative Access Team (HPCAT), X-ray Science Division, Argonne National Laboratory, Argonne, IL 60439, USA; hrubiak@anl.gov (R.H.); gyshe@anl.gov (G.S.); velisavljevi1@lnl.gov (N.V.)

³ Physics Division, Lawrence Livermore National Laboratory, Livermore, CA 94550, USA

* Correspondence: ykvohra@uab.edu

Abstract: The high-entropy transition metal borides containing a random distribution of five or more constituent metallic elements offer novel opportunities in designing materials that show crystalline phase stability, high strength, and thermal oxidation resistance under extreme conditions. We present a comprehensive theoretical and experimental investigation of prototypical high-entropy boride (HEB) materials such as (Hf, Mo, Nb, Ta, Ti)B₂ and (Hf, Mo, Nb, Ta, Zr)B₂ under extreme environments of pressures and temperatures. The theoretical tools include modeling elastic properties by special quasi-random structures that predict a bulk modulus of 288 GPa and a shear modulus of 215 GPa at ambient conditions. HEB samples were synthesized under high pressures and high temperatures and studied to 9.5 GPa and 2273 K in a large-volume pressure cell. The thermal equation of state measurement yielded a bulk modulus of 276 GPa, in excellent agreement with theory. The measured compressive yield strength by radial X-ray diffraction technique in a diamond anvil cell was 28 GPa at a pressure of 65 GPa, which is a significant fraction of the shear modulus at high pressures. The high compressive strength and phase stability of this material under high pressures and high temperatures make it an ideal candidate for application as a structural material in nuclear and aerospace fields.

Keywords: high pressure; high temperature; high-entropy materials; computational simulations; compressive strength



Citation: Iwan, S.; Lin, C.-M.; Perreault, C.; Chakrabarty, K.; Chen, C.-C.; Vohra, Y.; Hrubciak, R.; Shen, G.; Velisavljevic, N. High-Entropy Borides under Extreme Environment of Pressures and Temperatures. *Materials* **2022**, *15*, 3239. <https://doi.org/10.3390/ma15093239>

Academic Editor: Sergey V. Zharebtsov

Received: 27 March 2022

Accepted: 29 April 2022

Published: 30 April 2022

Publisher's Note: MDPI stays neutral with regard to jurisdictional claims in published maps and institutional affiliations.



Copyright: © 2022 by the authors. Licensee MDPI, Basel, Switzerland. This article is an open access article distributed under the terms and conditions of the Creative Commons Attribution (CC BY) license (<https://creativecommons.org/licenses/by/4.0/>).

1. Introduction

In a search for novel materials that retain their mechanical properties and oxidation resistance at high temperatures, transition metal borides have traditionally attracted increased attention [1]. This field of ultrahard and refractory materials has seen a new impetus recently due to the advent of high entropy materials that contain a random solid solution of five or more constituent elements [2–4]. Thus, one can envision a variety of high-entropy alloy, oxide, carbide, nitride, and boride materials that are stabilized by the high entropy of mixing given by $\Delta S_{\text{mix}} = R \ln(N)$, where R is the gas constant and N is the number of constituent elements. This high entropy of mixing also ensures that these materials are stable at high temperatures due to lower Gibb's free energy and can be exploited in applications where phase stability is an important materials selection criterion. Several high-entropy transition metal borides were synthesized recently [5], and their hardness and oxidation resistance were shown to be higher/better than the average performances of five individual metal diborides made by identical fabrication processing. Our motivation in this paper is to examine the structural and mechanical properties of high-entropy borides (HEBs) under combined high-pressure and high-temperature conditions, where materials synthesis and structural/compressibility measurements are combined in a single experiment [6]. In our

earlier study on the synthesis of (Hf, Mo, Zr, Ta, Ti) B_2 material (reported in [6]), the high-pressure high-temperature synthesized sample was not recovered at ambient conditions and, hence, only limited information on morphological, structural, element mapping, and mechanical properties could be gathered. We have addressed these shortcomings in the present study, where synthesized HEB samples have been recovered at ambient conditions for precise lattice parameter measurements, microstructure, characterization of residual phases, and subsequent shear strength measurements at high pressures in a diamond anvil cell. In addition, while a great deal of experimental data has been collected on HEB materials, the fundamental understanding of their entropy forming ability and structural and mechanical properties is still lacking due to difficulty in modeling disordered materials. We present a comprehensive theoretical and experimental investigation of prototypical high-entropy boride (HEB) materials such as (Hf, Mo, Nb, Ta, Ti) B_2 and (Hf, Mo, Nb, Ta, Zr) B_2 under combined high pressures and high temperatures and offer a detailed structural and mechanical characterization of these materials recovered from extreme environments. The (Hf, Mo, Nb, Ta, Ti) B_2 material was chosen for detailed high-pressure, high-temperature investigation because it is known to have the best thermal oxidation resistance of all the known transition metal borides up to 1200 °C [5], and our preliminary mechanical property measurements indicate that (Hf, Mo, Nb, Ta, Zr) B_2 has a high hardness value amongst HEB materials. In this study, we present a novel experimental approach where HEB material is synthesized under high pressures and high temperatures and its crystal structure and compressibility are studied under extreme environments in the same sample chamber without exposing the sample to ambient conditions, thereby minimizing contamination and generating data on high-purity HEB materials.

2. Materials and Methods

We performed density functional theory (DFT) calculations using the VASP software [7,8], which is based on a pseudopotential and plane-wave basis. We adopt the projector augmented wave (PAW) method [9,10] and the generalized gradient approximation (GGA) function based on Perdew-Burke-Ernzerhof (PBE) formalism [11]. The cutoff energy for the plane-wave basis was 446 eV, and the k-points were sampled by a Γ -centered Monkhorst-Pack mesh with a k-point density per reciprocal atom (KPPRA) \sim 10,000. The convergence criteria of electronic self-consistency and structural relaxation were set to 10 $^{-6}$ eV/unit cell and 10 $^{-3}$ eV/Å, respectively.

To model high-entropy materials, we further employed the stochastic (or special) quasi-random structure (SQS) [12]. SQS structures are traditionally generated by exhaustively enumerating all possible occupations of the sites in a supercell. However, its computation complexity grows exponentially with the supercell size, thereby suitable only for small unit cells (a few tens of atoms). Here, we utilize stochastic Monte Carlo approaches implemented in the Alloy Theoretic Automated Toolkit (ATAT) “mcsqs” code [13], which allows efficient generation of SQS structures over 100 atoms. After the SQS construction, we fully relaxed the structures under pressure up to 70 GPa. Afterwards, we further utilized the strain–stress method [14] implemented in VASP to compute the elastic constants C_{ij} , from which the bulk modulus K and shear modulus G can be evaluated using the Voigt-Reuss-Hill (VRH) average [15]. We note that the crystal symmetry of the original parent lattice can be reduced in SQS due to the presence of different atoms. In this case, a symmetrized C_{ij} , averaged over different directions, can be applied [16].

The high-pressure, high-temperature synthesis of HEB (Hf, Mo, Nb, Ta, Ti) B_2 and (Hf, Mo, Nb, Ta, Zr) B_2 samples was carried out at HPCAT beamline 16-BM-B [17] using a large volume Paris-Edinburgh (PE) press with a type of Cupped Drickamer Toroidal (CDT) cell. The synthesis process employed metal oxide precursors mixed with boron carbide and graphite that were high-energy ball-milled (Spex 8000M). CDT assembly is the newer cell being implemented with PE press at High Pressure Collaborative Access Team (HPCAT), and it provides more uniform (hydrostatic) pressure conditions and allows for extending experiments to higher pressure conditions (up to \sim 10 GPa). The beamline provides an in situ energy-dispersive X-ray diffraction (EDXD) probe during the synthesis

process as well as subsequent pressure–volume measurements to 9.5 GPa and 2273 K. The pressures were calibrated at high temperatures using the thermal equation of state for magnesium oxide [18] in the sample assembly, while the temperatures were established in a separate calibration of thermocouple measurement experiments and the power delivered to the graphite heater. The shear strength measurements on the (Hf, Mo, Nb, Ta, Ti)B₂ sample were carried out at HPCAT beamline 16-BM-D using radial angle-dispersive X-ray diffraction in a panoramic diamond anvil cell [19]. The secondary electron SEM images were acquired with a Quanta FEG 650 scanning electron microscope.

3. Results

3.1. Theoretical Results

Studying the mechanical properties of HEAs and HEBs is computationally challenging due to the extremely large phase space of possible compositions and systems that can be formed. It would be convenient if the elastic properties could be obtained using calculations on one single large-size supercell that effectively captures short-range correlation and efficiently mimics the randomness of high-entropy effects. Such approaches do exist, and we employ the SQS [12] approach in this paper. SQS represents the best periodic supercell that approximates a true disordered state for a given number of atoms. This is achieved by matching a specified set of correlations between neighboring sites to the corresponding correlation of a fully disordered state in the thermodynamic limit.

Figure 1 shows the SQS structures generated by Monte Carlo methods implemented in the ATAT-mcsqs code [13] for the hexagonal HEB (Hf, Mo, Nb, Ta, Ti)B₂. These structures of 135 and 150 atoms can be respectively regarded as $3 \times 3 \times 5$ and $5 \times 5 \times 2$ supercells of the parent lattice of hexagonal AlB₂ structure, but with the Al Wyckoff site replaced by five different metals with equal probability. ATAT-mcsqs allows the efficient generation of SQS structures over 100 atoms, and it is important to check different SQS sizes and shapes to ensure that physical properties of interests are converged and represent those in the thermodynamic limit.

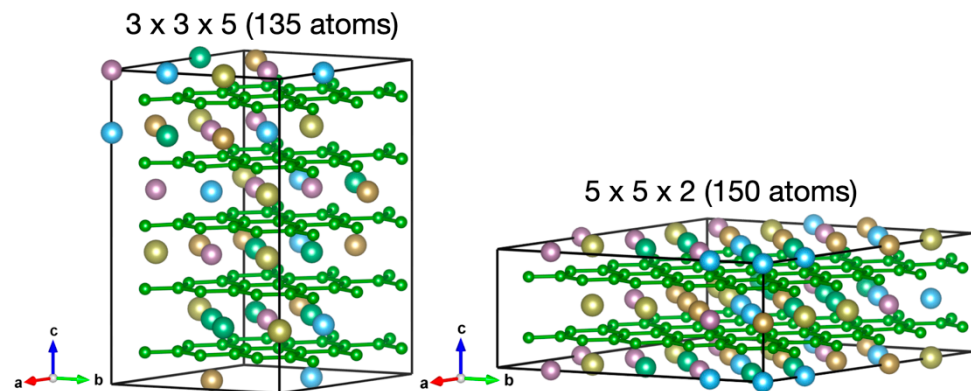


Figure 1. Special quasi-random structures (SQSs) for simulating the compression and mechanical behaviors of the hexagonal high-entropy boride (Hf, Mo, Nb, Ta, Ti)B₂. The SQS structures include 135 atoms (left) and 150 atoms (right), which, respectively, can be regarded as $3 \times 3 \times 5$ and $5 \times 5 \times 2$ supercells of the parent lattice of the hexagonal AlB₂ structure.

Figure 2a indicates that the volumes versus external pressure for different fully relaxed SQS structures agree extremely well. At ambient pressure, the volume of (Hf, Mo, Nb, Ta, Ti)B₂ from the 150-atom SQS structure (blue curve) is 27.47 Å³. This theoretically predicted volume is within 2% of the experimentally measured value of 26.882 Å³. Figure 2b shows the corresponding bulk and shear moduli as a function of pressure. In the 150-atom SQS results (blue curves), the ambient-pressure bulk and shear modulus values are, respectively, $K_0 = 288$ GPa and $G_0 = 215$ GPa. The theoretical value of K_0 is in good agreement with the experimentally determined $K_0 = 276$ GPa.

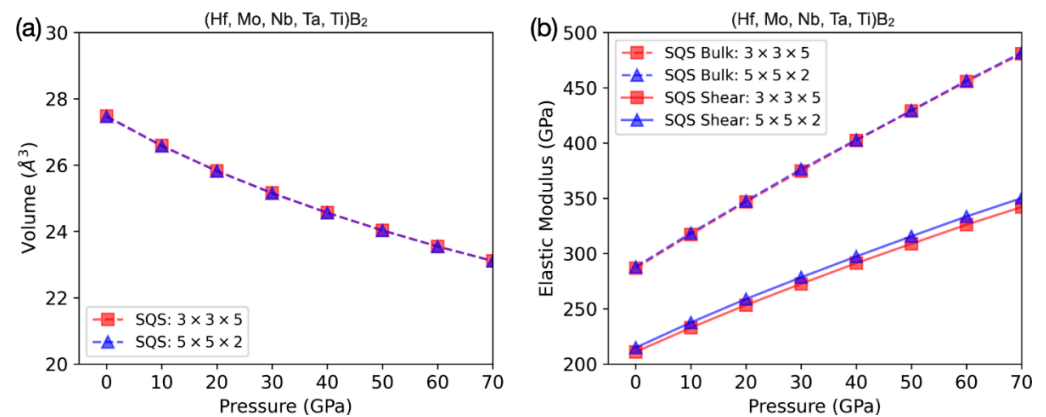


Figure 2. Volume and elastic moduli of different SQS structures computed for (Hf, Mo, Nb, Ta, Ti)B₂. (a) The computed volumes of the 135-atom (red square) and 150-atom (blue triangle) SQS structures match well with each other. (b) The bulk and shear moduli computed by both SQS structures are also in very good agreement. The theoretical bulk and shear moduli at zero pressure from the 150-atom SQS structure are $K_0 = 288$ GPa and $G_0 = 215$ GPa, respectively.

3.2. Experimental Results

The precursor materials contained equimolar amounts of five transition metal oxides: HfO₂, TiO₂, NbO₂, Ta₂O₅, MoO₃, Nb₂O₅, carbon black, and boron carbide from Alfa Aesar. First, the metal oxides combined with carbon were high-energy ball-milled (Spex 8000M) for two hours in a tungsten carbide container and media. At hourly intervals, the ball mill was allowed to cool for 10 min. The boron carbide was then added to the mixture to blend by ball mill with the milled metal oxides and carbon. To reduce contamination of tungsten carbide, the mixture with B₄C was wet-milled in acetone for four hours with zirconia balls. The mixture included an excess of B₄C (9% by weight) to account for the boron lost due to the formation of boron oxide and carbon monoxide, B₂O₃ and CO, during high-pressure, high-temperature synthesis [20]. The milled mixture was dried before being passed through a 200-mesh sieve to improve the uniformity of particle size for subsequent processing. Figure 3 shows the sample assembly and the synthesized sample recovered after the synthesis at high pressures and high temperatures.

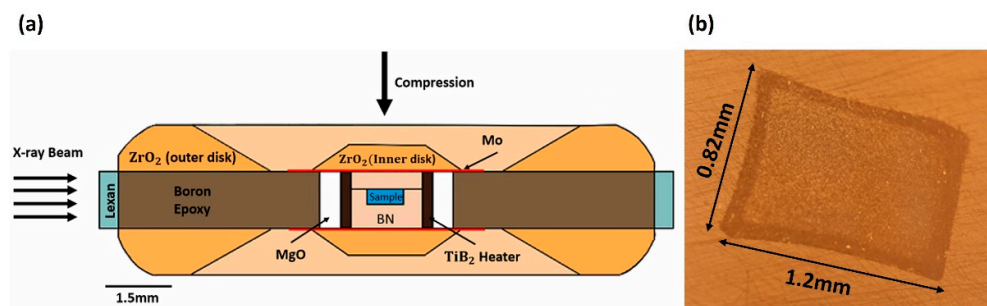


Figure 3. (a) Cupped Drickamer toroidal (CDT) employed in the high-pressure, high-temperature synthesis of high-entropy borides. The sample chamber contains a mixture of precursor materials depending on the desired composition. (b) The synthesized (Hf, Mo, Nb, Ta, Ti)B₂ sample of 1.2 × 0.82 mm was recovered for a detailed characterization of its physical and mechanical properties, as described in the text.

The sample recovered at ambient conditions after high-pressure, high-temperature synthesis was analyzed by angle dispersive X-ray diffraction (ADX) to confirm that the single hexagonal AlB₂ phase was observed with no WC-Co or ZrO₂ contamination. Figure 4 shows ADXD patterns for both (Hf, Mo, Nb, Ta, Ti)B₂ and (Hf, Mo, Nb, Ta, Zr)B₂ samples, showing

the single hexagonal AlB_2 phase with no contaminants from the ball milling process. There is only a remanent BN phase from the sample container at the edges of the sample, along with a very weak amount of unreacted hafnium dioxide in one case. The measured ambient lattice parameters for $(Hf, Mo, Nb, Ta, Ti)B_2$ are $a = 3.0746 \text{ \AA}$, $c = 3.2837 \text{ \AA}$, with unit cell volume $V_0 = 26.882 \text{ \AA}^3$. The measured ambient lattice parameters for $(Hf, Mo, Nb, Ta, Zr)B_2$ are $a = 3.1037 \text{ \AA}$, $c = 3.3822 \text{ \AA}$, with unit cell volume $V_0 = 28.216 \text{ \AA}^3$.

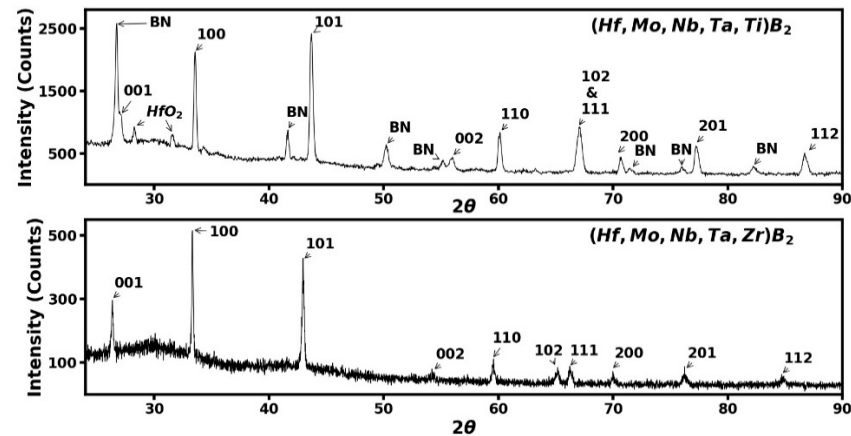


Figure 4. The angle-dispersive X-ray diffraction spectra for the two samples at ambient conditions after synthesis at high pressures and high temperatures. Both samples show a single hexagonal AlB_2 phase with ten diffraction peaks labeled with (hkl) values; no contaminants were detected. The peaks marked BN come from the sample container used in the synthesis process and very weak unreacted hafnium oxide in the upper panel.

Scanning electron microscopy (SEM) and energy dispersive spectroscopy (EDS) were performed to ascertain the uniform distribution of elements in the high entropy boride. Figure 5 shows the SEM image and the EDS analysis showing the distribution of the five transition metals and boron throughout the bulk of the sample, confirming single-phase observation by X-ray diffraction. Further high-resolution EDS and nanoscale composition mapping studies will be needed to establish uniform compositions from nanoscale to microscale. The additional information on grain size is provided by a higher-resolution SEM image in Figure 6, which shows an average grain size of two microns. The high-pressure, high-temperature synthesized sample was studied up to 9.5 GPa and 2273 K, and the energy dispersive X-ray diffraction pattern is shown in Figure 7. The hexagonal AlB_2 structure was stable to the highest pressure and temperature reached in this study, as evidenced by the strong (110) , (012) , (020) , (021) , (112) , (022) , $(013)/(120)$, (121) , and (030) distinct Bragg diffraction peaks from this structure, which are clearly visible in addition to the X-ray fluorescence peaks from the constituent elements (Figure 7). The measured lattice parameters for the hexagonal AlB_2 phase at 9.5 GPa and 2273 K are $a = 3.0886 \text{ \AA}$ and $c = 3.2807 \text{ \AA}$.

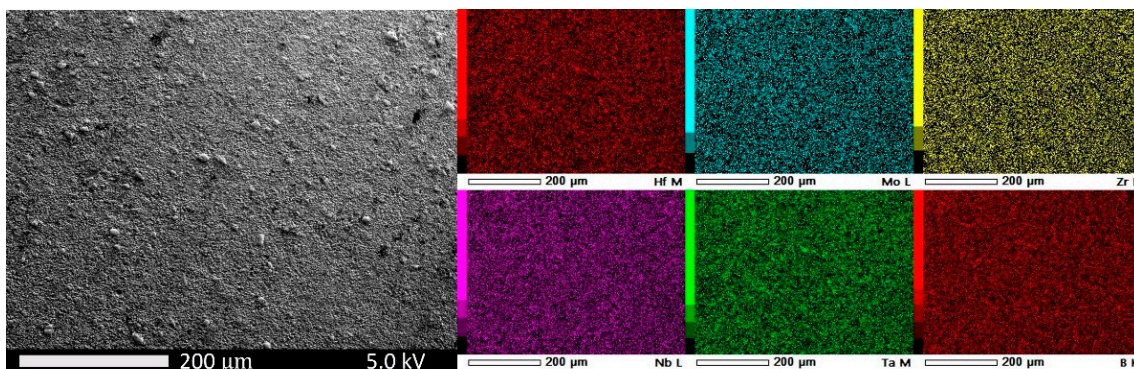


Figure 5. SEM and EDS analysis of high-pressure, high-temperature synthesized (Hf, Mo, Nb, Ta, Zr)B₂ sample. The EDS analysis based on X-ray fluorescence shows the distribution of the five transition metals and boron in the high entropy boride sample.

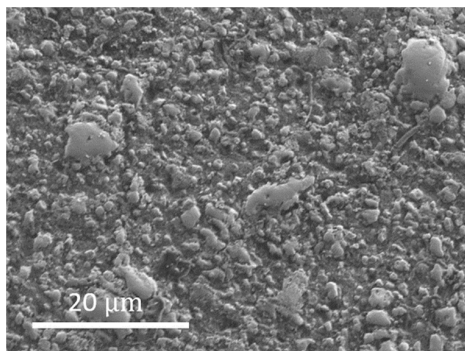


Figure 6. High-resolution SEM image of the (Hf, Mo, Nb, Ta, Zr)B₂ sample showing an average grain size of 2 microns. The few large grains observed in this micrograph are also from the (Hf, Mo, Nb, Ta, Zr)B₂ sample.

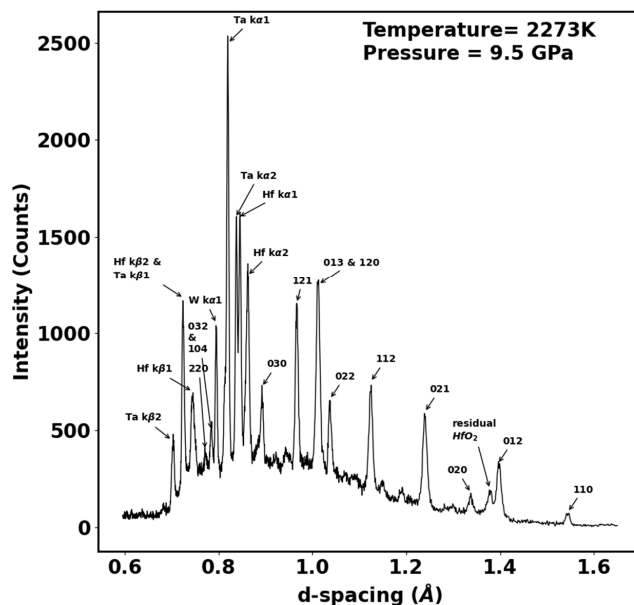


Figure 7. Energy-dispersive X-ray diffraction spectrum of the (Hf, Mo, Nb, Ta, Ti)B₂ sample at a pressure of 9.5 GPa and temperature of 2273 K. The sample peaks are indexed to a hexagonal AlB₂ phase, with lattice parameters described in the text, along with the fluorescence peaks from the constituent elements. A weak peak from residual precursor material hafnium dioxide is also indicated.

A series of high-temperature heating runs were conducted to map out the P-V-T space for this material. The decompression data was also collected at ambient temperature to establish the room-temperature equation of state. The combined data set is shown in Figure 8. The 2nd Order Birch Murnaghan equation of state (BM EoS) in Equation (1) was used with the thermal expansion model [21,22] shown in Equation (2) to extract the bulk modulus (K_0), dK/dT , and the volumetric thermal expansion coefficient α .

$$P(V) = \frac{3}{2}K_0 \left[x^{\frac{7}{3}} - x^{\frac{5}{3}} \right] \left[1 + \frac{3}{4}(K_0' - 4)(x^{\frac{2}{3}} - 1) \right] \quad (1)$$

$$V_{0T} = V_{00} \exp \left(\alpha_0 (T - T_{ref}) + \frac{1}{2} \alpha_1 (T^2 - T_{ref}^2) + \alpha_2 \left(\frac{1}{T} - \frac{1}{T_{ref}} \right) \right) \quad (2)$$

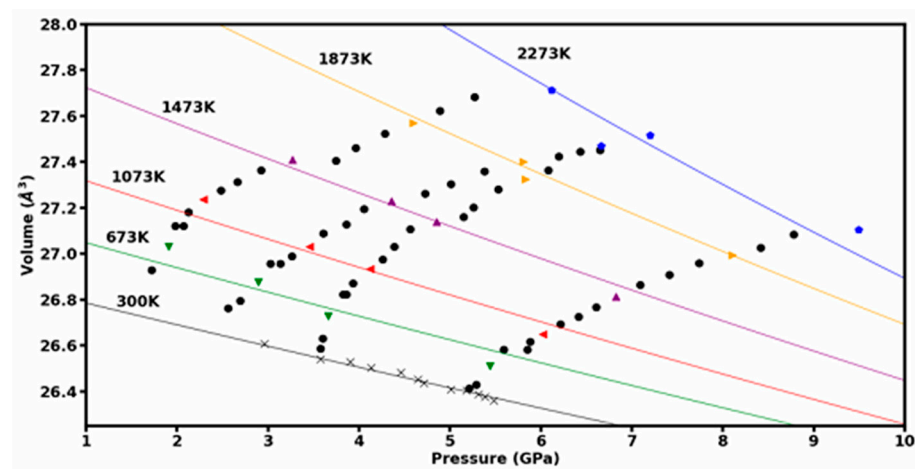


Figure 8. The measured Pressure–Volume–Temperature data for the (Hf, Mo, Nb, Ta, Ti) B_2 sample to 9.5 GPa and 2273 K. The “x” marked data points were taken during decompression at 300 K. The solid lines are fitted to various isotherms ranging from 300 to 2273 K. The thermal equation of state fit is described in the text.

In Equation (1), $x = V_0/V$, K_0 is the bulk modulus, and K_0' is the first pressure derivative. For Equation (2), the temperature-dependent volumetric thermal expansion α is described by coefficients α_0 , α_1 , α_2 as $\alpha = \alpha_0 + \alpha_1 T + \alpha_2 T^{-2}$. The fit to P-V-T data shown in Figure 8 yields information on the thermoelastic properties of the synthesized HEB sample. Using the ambient pressure unit-cell volume measured earlier $V_0 = 26.882 \text{ \AA}^3$, the fit resulted in a bulk modulus $K_0 = 276 \text{ GPa}$ at ambient temperature with a fixed value of $K_0' = 4$. The fitted value of the temperature derivative of bulk modulus is $dK/dT = -0.090 \text{ GPa/K}$. Thermal expansion coefficients were calculated to be $\alpha_0 = -1.533 \times 10^{-5} \text{ K}^{-1}$, $\alpha_1 = 4.071 \times 10^{-8} \text{ K}^{-2}$, and $\alpha_2 = 4.60 \text{ K}$, with the volumetric thermal expansion expressed as $\alpha = \alpha_0 + \alpha_1 T + \alpha_2 T^{-2}$ in the temperature range between 300 and 2300 K.

The radial X-ray diffraction data on the HEB sample was collected to 65 GPa using platinum as an X-ray pressure standard. Collected radial X-ray diffraction patterns were integrated into 72 azimuthal segments of $\delta = 5$ degrees around the entire pattern using the methodology described in [19]. The measured d-spacing (d_m) of the HEB sample for each 5-degree segment can be obtained using Equation (3):

$$d_m(hkl) = d_p + d_p Q_{hkl} (1 - 3 \cos^2 \chi) \quad (3)$$

where d_p is the hydrostatic component of compression, Q_{hkl} is the lattice strain, and χ is the angle between the DAC compression axis and the diffraction plane normal defined by $\cos \chi = \cos \delta \cos \theta$. The linear relationship between measured d-spacing d_m and the $1 - 3 \cos^2 \chi$ term allows for direct calculation of the estimated hydrostatic d-spacing d_p by eliminating the directionally dependent lattice strain Q_{hkl} term when $1 - 3 \cos^2 \chi = 0$.

When lattice strain Q_{hkl} is present in a sample, the differential stress t , which is a measure of compressive yield strength [23] of the material, can be determined by averaging the strain over all hkl and using Equation (4). Furthermore, differential stress t is approximately twice the shear strength τ of the material.

$$6\langle Q_{hkl} \rangle = \frac{t}{G}, \quad t = 2\tau \quad (4)$$

where G is the sample shear modulus.

Figure 9 shows the angle dispersive X-ray diffraction spectrum of the (Hf, Mo, Nb, Ta, Ti) B_2 sample mixed with the platinum pressure marker at a pressure of 65 GPa. The variation in the 2-Theta diffraction angle along the azimuthal angle shows the effect of the differential stress supported by the sample. In contrast to the (Hf, Mo, Nb, Ta, Ti) B_2 sample, the platinum pressure marker shows relatively less variation in the 2-Theta angle along the azimuthal angle. The lattice strain Q_{hkl} is then averaged from the observed hkl peaks and used in Equation (4) to determine the compressive strength using the computed value of shear modulus. The differential stress t normalized to shear modulus (G) is plotted in Figure 10, with the hydrostatic pressure values obtained from the platinum marker. The experimentally measured differential stress t (or compressive strength) is observed to increase with increasing pressure and approaches a value as high as 8% of shear modulus at 65 GPa. Using the theoretical value of shear modulus at 65 GPa, the compressive strength of the (Hf, Mo, Nb, Ta, Ti) B_2 sample is estimated to be as high as 28 GPa.

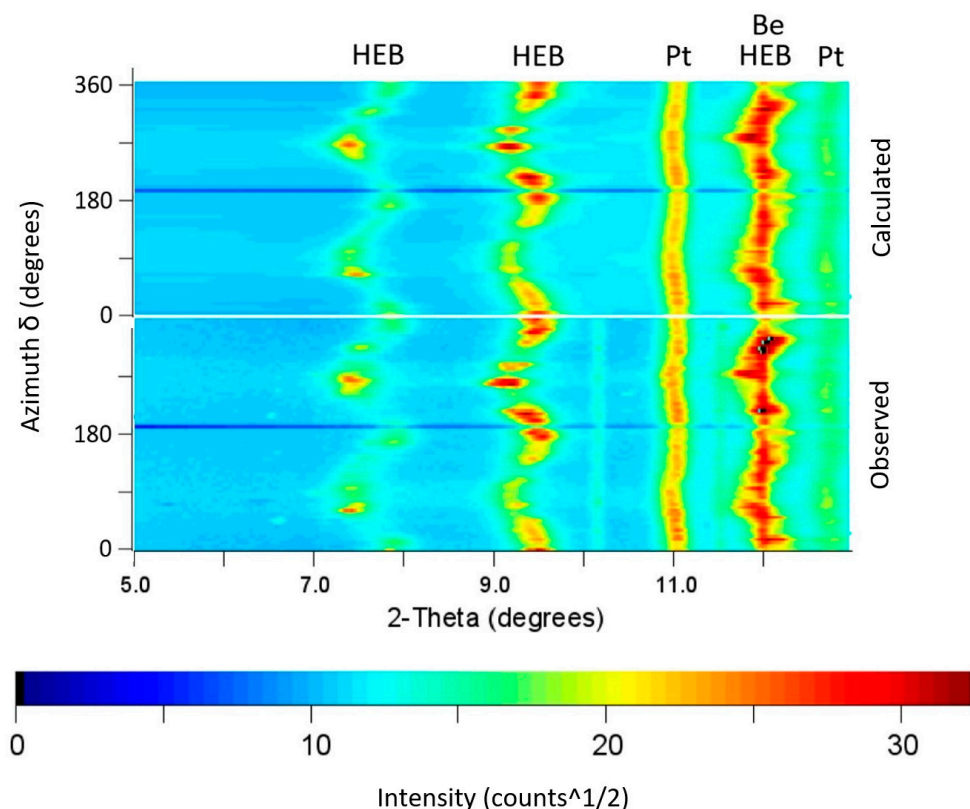


Figure 9. The X-ray diffraction pattern of the HEB sample (Hf, Mo, Nb, Ta, Ti) B_2 along with platinum (Pt) marker at a pressure of 65 GPa in a radial diffraction mode with beryllium (Be) gasket. The waviness in the diffraction lines reflects the large anisotropy in elastic strains present for a high-strength material such as HEB compared to a platinum pressure marker. The lower panel shows the observed diffraction intensities in the azimuthal direction, while the upper panel shows the calculated intensities.

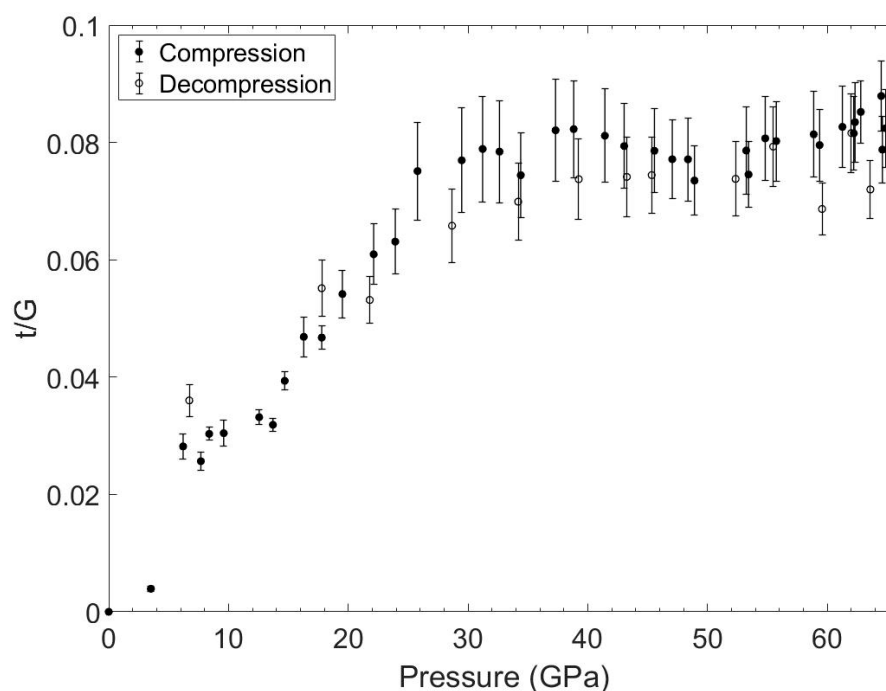


Figure 10. The measured value of differential stress (t) normalized to shear modulus for HEB (Hf, Mo, Nb, Ta, Ti) B_2 sample to 65 GPa. The data are shown for both compression and decompression cycles. The HEB sample shows high differential stress, approaching 8% of the shear modulus.

4. Discussion

The HEB samples were synthesized under high pressures and high temperatures, starting from ball-milled oxide precursors mixed with boron carbide and graphite powders. The reduction of grain size of precursor materials using ball-milling led to rapid transformation in several minutes to HEB under high pressures and high temperatures; however, transformation kinetics was not the focus of this study. The experimental approach, where HEB material is synthesized under high pressures and high temperatures and its crystal structure and compressibility are studied under extreme environments in the same sample chamber without exposing the sample to ambient conditions, has yielded crystal structure data, the thermal equation of state data, and compressive yield strength data on high-entropy transition metal boride materials. The hexagonal AlB_2 phase of the high-entropy transition metal boride sample is stable to the extreme high pressures and high temperatures achieved in this study. The measured value of bulk-modulus for (Hf, Mo, Nb, Ta, Ti) B_2 is $K_0 = 276$ GPa and is in good agreement with the theoretically predicted value of $K_0 = 288$ GPa in this study. The measured value of $K_0 = 276$ GPa for (Hf, Mo, Nb, Ta, Ti) B_2 is lower than the reported value of $K_0 = 344$ GPa for (Hf, Mo, Zr, Ta, Ti) B_2 [6]; however, the ambient pressure volume was not directly measured in the earlier study and that could impact the determination of bulk-modulus in [6]. The measured high compressive yield strength of HEB materials at high pressures is also supported by a theoretical model that predicts an increase in shear modulus with increasing pressure. The measured compressive yield strength of HEB is 8% of shear modulus (G) at 65 GPa. The shear strength τ is approximately half of compressive yield strength and is estimated to be about $0.04 G$ at 65 GPa. The theoretical estimate of τ is $G/6$ [19] or $0.167 G$ is four times higher than the experimental value. This difference is likely since crystal imperfections are not included in the theoretical models of HEB, and more realistic models are needed for better comparison with experimental shear strength data.

5. Conclusions

We present a comprehensive theoretical and experimental study of the compression and deformation behavior of prototypical high-entropy transition metal boride (Hf, Mo, Nb, Ta, Ti) B_2 and (Hf, Mo, Nb, Ta, Zr) B_2 samples to high pressures and high temperatures. The high-pressure, high-temperature synthesis and compression studies of high-entropy transition metal borides are carried out in the same sample chamber, thereby minimizing exposure to ambient environments. The hexagonal AlB_2 phase of both high-entropy boride samples was found to be stable to pressure and temperature conditions of 9.5 GPa and 2273 K, respectively. The supercell approach using the stochastic (or special) quasi-random structure (SQS) predicts a bulk modulus value of 288 GPa, in excellent agreement with the measured value of 276 GPa. The changes in bulk modulus and thermal expansion coefficient with temperatures were also documented in this study. The compressive strength of the (Hf, Mo, Nb, Ta, Ti) B_2 sample approaches a value of 28 GPa at an applied pressure of 65 GPa in a measurement carried out in a diamond anvil cell. The high compressive strength and phase stability of this material under high pressures and high temperatures make it an ideal candidate for application as a structural material in nuclear and aerospace fields.

Author Contributions: Conceptualization, Y.V. and C.-C.C.; methodology, S.I., R.H., G.S., N.V. and K.C.; software, C.-M.L. and C.-C.C.; formal analysis, S.I., C.P. and C.-M.L.; resources, N.V.; data curation, S.I.; writing—review and editing, Y.V., S.I. and C.-C.C.; supervision, Y.V. and C.-C.C.; funding acquisition, Y.V. All authors have read and agreed to the published version of the manuscript.

Funding: This material is based upon work supported by the Department of Energy, National Nuclear Security Administration, under Award Number DE-NA0003916.

Institutional Review Board Statement: Not applicable.

Informed Consent Statement: Not applicable.

Data Availability Statement: All data generated or analyzed and materials synthesized during this study are included in this published article. Additional raw data used and/or analyzed during the current study are available from the corresponding author upon reasonable request.

Acknowledgments: Seth Iwan would like to acknowledge Graduate Fellowship support under the NASA/Alabama Space Grant Consortium (Grant No. NNH19ZHA001C) and summer internship support from HPCAT, Argonne National Laboratory. Portions of this work were performed at HPCAT (Sector 16), Advanced Photon Source (APS), and Argonne National Laboratory. HPCAT operations are supported by DOE-NNSA's Office of Experimental Sciences. The Advanced Photon Source is a U.S. Department of Energy (DOE) Office of Science User Facility operated for the DOE Office of Science by Argonne National Laboratory under Contract No. DE-AC02-06CH11357. NV work was performed under the auspices of the U.S. Department of Energy by Lawrence Livermore National Laboratory under Contract DE-AC52-07NA27344. The calculations were performed on the Frontera computing system at the Texas Advanced Computing Center. Frontera is made possible by NSF award OAC-1818253.

Conflicts of Interest: The authors declare no conflict of interest.

References

1. Al-Jothery, H.K.M.; Albarody, T.M.B.; Yusoff, P.S.M.; Abdullah, M.A.; Hussein, A.R. A review of ultra-high temperature materials for thermal protection system. In Proceedings of the IOP Conference Series: Materials Science and Engineering, Kuantan, Malaysia, 1–2 October 2019; Volume 863, p. 012003.
2. George, E.P.; Raabe, D.; Ritchie, R.O. High-entropy alloys. *Nat. Rev. Mater.* **2019**, *4*, 515. [[CrossRef](#)]
3. Zhang, Y.; Zuo, T.; Tang, Z.; Gao, M.; Dahmen, K.; Liaw, P.; Lu, Z. Microstructures and properties of high-entropy alloys. *Prog. Mater. Sci.* **2014**, *61*, 1–93. [[CrossRef](#)]
4. Ishizu, N.; Kitawaga, J. New high-entropy alloy superconductor Hf₂₁Nb₂₅Ti₁₅V₁₅Zr₂₄. *Results Phys.* **2019**, *13*, 102275. [[CrossRef](#)]
5. Gild, J.; Zhang, Y.; Harrington, T.; Jiang, S.; Hu, T.; Quinn, M.C.; Mellor, W.M.; Zhou, N.; Vecchio, K.; Luo, J. High-Entropy Metal Diborides: A New Class of High-Entropy Materials and a New Type of Ultrahigh Temperature Ceramics. *Sci. Rep.* **2016**, *6*, 37946. [[CrossRef](#)] [[PubMed](#)]
6. Iwan, S.; Burrage, K.C.; Storr, B.C.; Catledge, S.A.; Vohra, Y.K.; Hrubiak, R.; Velisavljevic, N. High-pressure high-temperature synthesis, and thermal equation of state of high-entropy transition metal boride. *AIP Adv.* **2021**, *11*, 035107. [[CrossRef](#)]

7. Kresse, G.; Furthmüller, J. Efficiency of ab-initio total energy calculations for metals and semiconductors using a plane-wave basis set. *Comput. Mater. Sci.* **1996**, *6*, 15–50. [[CrossRef](#)]
8. Kresse, G.; Furthmüller, J. Efficient iterative schemes for ab initio total-energy calculations using a plane-wave basis set. *Phys. Rev. B* **1996**, *54*, 11169. [[CrossRef](#)] [[PubMed](#)]
9. Blöchl, P.E. Projector augmented-wave method. *Phys. Rev. B* **1994**, *50*, 17953. [[CrossRef](#)] [[PubMed](#)]
10. Kresse, G.; Joubert, D. From ultrasoft pseudopotentials to the projector augmented-wave method. *Phys. Rev. B* **1999**, *59*, 1758. [[CrossRef](#)]
11. Perdew, J.P.; Burke, K.; Ernzerhof, M. Generalized Gradient Approximation Made Simple. *Phys. Rev. Lett.* **1997**, *77*, 3865. [[CrossRef](#)] [[PubMed](#)]
12. Zunger, A.; Wei, S.-H.; Ferreira, L.G.; Bernard, J.E. Special quasirandom structures. *Phys. Rev. Lett.* **1990**, *65*, 353. [[CrossRef](#)] [[PubMed](#)]
13. Van de Walle, A.; Tiwary, P.; De Jong, M.; Olmsted, D.L.; Asta, M.; Dick, A.; Shin, D.; Wang, Y.; Chen, L.Q.; Liu, Z.K. Efficient stochastic generation of special quasirandom structures. *Calphad* **2013**, *42*, 13–18. [[CrossRef](#)]
14. Le Page, Y. and Saxe, Symmetry-general least-squares extraction of elastic data for strained materials from ab initio calculations of stress. *Phys. Rev. B* **2002**, *65*, 104104. [[CrossRef](#)]
15. Hill, R. The elastic behaviour of a crystalline aggregate. *Proc. Phys. Soc. Sect. A* **1952**, *65*, 349. [[CrossRef](#)]
16. Huang, Z.; Liu, G.; Zhang, B.; Yan, M.; Fu, Y. A theoretical study of the stability, mechanical and thermal properties of AlNiCuCo equimolar high entropy alloy. *Phys. Lett. A* **2020**, *384*, 126797. [[CrossRef](#)]
17. Kono, Y.; Park, C.; Kenney-Benson, C.; Shen, G.; Wang, Y. Toward comprehensive studies of liquids at high pressures and high temperatures: Combined structure, elastic wave velocity, and viscosity measurements in the Paris–Edinburgh cell. *Phys. Earth Planet. Inter.* **2014**, *228*, 269. [[CrossRef](#)]
18. Kono, Y.; Irifune, T.; Higo, Y.; Inoue, T.; Barnhoorn, A. P-V-T relation of MgO derived by simultaneous elastic wave velocity and in situ X-ray measurements: A new pressure scale for the mantle transition region. *Phys. Earth Planet. Inter.* **2010**, *183*, 211. [[CrossRef](#)]
19. Burrage, K.C.; Changyong, P.; Vohra, Y.K. Shear strength measurements and hydrostatic compression of rhenium diboride under high pressures. *J. Appl. Phys.* **2021**, *129*, 205901. [[CrossRef](#)]
20. Feng, L.; Fahrenholtz, W.G.; Hilmas, G.E. Two-step synthesis process for high-entropy diboride powders. *J. Am. Ceram. Soc.* **2019**, *103*, 724. [[CrossRef](#)]
21. Fei, Y. Thermal Expansion. In *Mineral Physics & Crystallography*; American Geophysical Union (AGU): Washington DC, USA, 2013; pp. 29–44.
22. Anderson, O.L. *Equations of State of Solids for Geophysics and Ceramic Science*; Oxford University Press: Oxford, UK, 1995.
23. Shen, G.; Mao, H.K. High-pressure studies with X-rays using diamond anvil cells. *Rep. Prog. Phys.* **2017**, *80*, 016101. [[CrossRef](#)] [[PubMed](#)]